2006. The ride comfort and energy-regenerative characteristics analysis of hydraulic-electricity energy regenerative suspension

Bian Gong[1], Xuexun Guo[2], Sanbao Hu[3], Zhigang Fang[4]
School of Automotive Engineering, Hubei Key Laboratory of Advanced Technology of Automotive Parts,
Hubei Collaborative Innovation Center for Automotive Components Technology,
Wuhan University of Technology, Wuhan 430070, China
[3]Corresponding author
E-mail: [1]*gbjeason@163.com*, [2]*guo6531@163.com*, [3]*autogb@126.com*, [4]*zuoleng136@163.com*

Abstract. For optimization of performances of a hydraulic-electricity energy regenerative suspension (HERS) unit, the tradeoff point was determined based on study of ride comfort and energy-regenerative characteristics of a HERS unit in this study. A HERS unit as a new energy reclaiming suspension device is equipped with an energy-harvesting hydraulic electromagnetic shock absorber (HESA). The HESA together with a quarter car was modeled based on theoretical analysis and experiments, in which the root mean square (RMS) values of the sprung mass vibration acceleration and the recovered power are regarded as the optimization objectives under different road excitation conditions such as the constraints (natural frequency, dynamic displacement, and dynamic load of wheels). The HERS unit was optimized after the relationship between the ride comfort and the energy regeneration was obtained. In comparison with the traditional suspension, the HERS unit may be utilized to improve the ride comfort and meet the vehicle-driving requirements. Moreover, the total input power may be saved by 34-100 W on average while the vibration acceleration is among 0.65-1.06 m/s^2. Furthermore, it is verified that the HERS damping force control is the feasible under various load currents.

Keywords: hydraulic-electricity energy regenerative suspension, ride comfort, energy-regenerative, optimization.

1. Introduction

70 % of oil consumption is used for transportation (DOE data [1]) in the United States, in which automobiles make up 62 % [1, 2]. On the other hand, only 10 %-16 % of the available fuel energy is used for vehicle-driving (DOE and EPA data [3]).

The kinetic energy is primarily dissipated due to vehicle vibration and motion for a car. As for traditional viscous shock absorbers, the excitation energy is dissipated passively into waste heat due to road irregularity and the transferred vibration might cause discomfort of passengers; thus, some effective measures should be taken to recover such considerable amount of kinetic energy dissipated in conventional vehicle suspension shock absorbers.

A great deal of research work was carried out to recycle such potential kinetic energy dissipation. Karnapp made variable vehicle suspension mechanical dampers including permanent magnet linear motors to change the external resistance [4]. Hsu indicated that driving, road conditions and the control algorithm were primary influencing factors for the recoverable energy and the active suspension may affect the suspension performances to some extent while recycling energy [5]. Suda et al. developed a self-powered active suspension unit with two linear DC motors (one as an energy regenerative damper recycling the kinetic energy; and the other one as an actuator) and the corresponding tests proved that their hybrid suspension unit may improve the isolation performance especially at high frequency [6]; moreover, one linear DC motor may also be used to realize the active control and energy recovery [7, 8]. Kawamoto et al. put forward an active suspension scheme integrating a ball screw mechanism and an electro-mechanical actuator, whose measured results indicate the regenerated power is 33 W [9]. Chen investigated a

self-sensing magnetorheological (MR) damper for power generation to integrate energy harvesting, dynamic sensing and MR damping technologies [10].

Energy-harvesting shock absorbers having the potential of converting kinetic energy into electric power have been being is one of the research hotspots in both academia and industry for more than two decades. The semi-active suspension scheme was put forward to better compromise between energy consumption and suspension performances. There are various regenerative shock absorbers such as electromagnetic and regenerative hydraulic suspension units based on different operating principles and design schemes. The energy-harvesting shock absorbers are primarily classified into linear and rotary harvesters in accordance with motion modes of energy generators; the former is a linear generator in shape of a shock absorber to generate electricity due to relative linear motion between magnets and coils. An active damper including a linear motor for changing very rapidly the damping ratio was developed in Bose Corp; and measured results show that the suspension unit equipped with an active damper give rise to smoother ride [11]. Zuo et al. [12] designed a linear electromagnetic energy harvester to efficiently recover the vibration energy in a compact space. The prototype test results revealed that the harvester may generate energy (more than 16-64 W) per shock absorber while the RMS suspension velocity is 0.25-0.5 m/s. On the other hand, the latter being made up of hydraulic, ball-screw, and rack-pinion mechanisms as one type of electromagnetic regenerative shock absorbers takes advantages of a better price/performance ratio and smaller sizes; and the linear suspension motion may be converted into the rotary movement in generators.

Kawamoto Y. presented an electromagnetic damper including a DC motor, a ball screw and a nut, in which the linear motion is converted to rotary motion by the ball screw and the nut [13]. Zhang et al. designed a motor actuator prototype including a ball-screw mechanism and an energy-regenerative suspension mechanism [14], whose test results indicated that good shock isolation effects may be achieved under low-frequency road excitation conditions; however, such ball-screw motion converter resulted in poor performances and low efficiency at high frequencies.

Choi developed a rack and pinion mechanism to convert piston's linear motion to rotary motion to improve the vibration isolation characteristics of the ball-screw harvester at high frequencies [15]. Li presented a regenerative shock absorber including a rack and pinion mechanism [16], in which a gearbox is equipped to increase rotational speed. However, backlash, friction and bevel gears lower its efficiency but increase its cost represents such mechanism.

A hydraulic motor is connected with an electric generator in a hydraulic regenerative shock absorber. A hydraulic rectifier bridge is used to convert reciprocating oil flowing of the damper into the unidirectional rotation of the hydraulic motor so that the vibration energy due to road irregularity may be absorbed represents supply of the damping effect [17]. Fang presented a new kind of shock absorber (namely a hydraulic electromagnetic shock absorber (HESA)) and the detailed analysis was carried out to its damping and energy regeneration characteristics; moreover, its prototype test results indicate that about 200 W may be recovered under the excitation conditions (3 mm and 10 Hz) [18]. Zhang studied the suspension performance effects of HESA and found the most remarkable influencing factor of the energy regenerative suspension unit; however, there is not any result in comparison with those of a traditional suspension unit [19].

A HESA (new energy regenerative suspension unit) is primarily to reduce the vibration disturbance from road roughness, acceleration/deceleration, and cornering to the chassis represents better ride comfort and good tire-ground contact force represents better vehicle handling and mobility, represents replacement of conventional shock absorbers and matching the vehicle perfectly, comparison between HESA and traditional absorbers was carried out in this study. Moreover, HESA was optimized by utilizing the multi-objective optimization method. The experimental verification was carried out to achieve better compromise between the ride comfort and the energy regeneration characteristics.

2. Modeling HERS

2.1. HESA model

HESA as a new kind of rotary regenerative shock absorbers may not only isolate vibration but also recover a part of energy dissipation, whose operating principle was presented in detail by Fang [18]; moreover, there is no significant difference in damping effects between the jounce and rebound strokes.
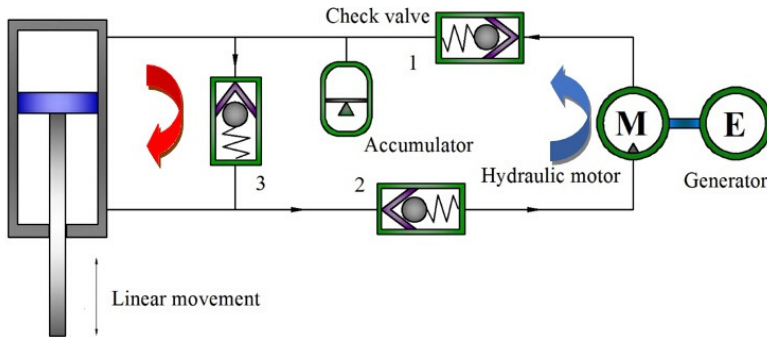

Fig. 1. Schematic diagram of a HESA unit

Thus, improvement was carried out to meet the vehicle shock absorption requirement. The new structure of HESA is shown in Fig. 1, which is composed of a hydraulic cylinder, check valves, accumulator, a hydraulic motor, a generator, and pipelines and so on and Where: the red and blue arrows indicate fluid flows in jounce and rebound strokes, respectively. The compression damping force should be smaller than the expansion one according to the vehicle shock absorption demand. The current HESA structure contributes to satisfy the demand based on various hydraulic circuits. The target vehicle's shock absorber was reprocessed based on the operating principle of HESA, whose schematic diagram is shown in Fig. 2 and whose rebound valve (on the piston) rather than other valves is removed. The original piston rod is replaced with a hollow bar whose lower end is connected with the upper operating chamber to transfer oil from the upper operating chamber. In addition, the connecting holes are designed in the bottom of the storage tank and the upper end of the piston rod, to connect any external motor-generator system.

When the body moves downwards, the lower operating chamber B is pressurized so that a part of oil may flow into the upper operating chamber through the flow valve on the piston. Due to there being a piston rod in the operating chamber A, other oil flows into the compensation chamber C through the compression valve and the same oil flowing path as the that during the compression process represents a traditional shock absorber.

The compression damping force occurs in the compression stroke, when upper operating chamber A is pressurized while the body moves upwards so that oil may flow into the external energy recovery system through the hollow piston rod and the hydraulic motor may be driven from the compensation chamber C to the lower operating chamber B. Due to there being no rebound valve, the damping force is chiefly provided by the external motor-generator system during rebound stroke.

In conclusion, HESA works as a traditional shock absorber when its piston moves downwards; on the other hand, the damping force is not only similar to that of an ordinary damper in this process but also provide the damping force represents isolating vibration and recycling a part of vibration energy while the piston moves upwards.

It is found that the rebound damping force dominate major differences in major mechanical differences based on the previous analysis; however, the damping force is primarily from hydraulic pipelines, check valves and the motor-generator system in a HESA while the local

pressure loss is neglected. While ignoring the internal leakage of the oil cylinder and the pressure of the compensation valve, the following pressure balance equation may be obtained to the upper operating chamber under high pressure in expansion stroke:

$$P_A = P_B + \Delta P_1 + \Delta P_e + \Delta P_2 + \Delta P_p, \tag{1}$$

where: P_A represents the pressure of the upper operating chamber; P_B represents the pressure of the lower operating chamber, ΔP_i represents the pressure drop of the check valve i ($i = 1, 2$); ΔP_e represents the pressure drop of a hydraulic motor; and ΔP_p represents the pressure drop of a hydraulic pipe.
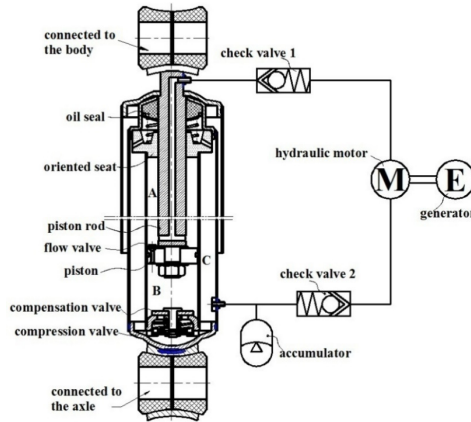

Fig. 2. Plane diagram of a HESA prototype

While ignoring the fiction force between the piston and the cylinder wall, the damping force may be expressed by:

$$F_c = P_A \cdot A_a - P_B \cdot A, \tag{2}$$

where: F_c represents the damping force in the expansion stroke; A_a represents the piston ring area on the side of the upper operating chamber; and A represents the piston cross-sectional area.

While neglecting the pressure drop of any compensation valve, the following equation comes into existence for P_B and P_{acc}:

$$P_B = P_{acc}, \tag{3}$$

where: P_{acc} represents the pressure of an accumulator.

Thus, the following equation may be obtained:

$$F_c = \left(\Delta P_1 + \Delta P_2 + \Delta P_e + \Delta P_p \right) \cdot A_a - P_{acc} \cdot A_r, \tag{4}$$

where: A_r represents the cross-sectional area of a piston rod, $A_r = A - A_a$.

While simplifying a check valve as a thin wall orifice, the pressure drop of a check valve may be calculated by:

$$Q_i = A_{ci} c_q \sqrt{\frac{2\Delta P_i}{\rho}}, \tag{5}$$

where: Q_i represents the oil flowrate of the check valve i ($i = 1, 2$), A_{ci} represents the orifice area of

the check valve i; c_q represents the oil flow coefficient ($c_q = 0.6$); and ρ represents the oil density.

Then, the pressure drop of a check valve may be expressed as follows:

$$\Delta P_i = \frac{\rho}{2c_q^2 A_{ci}^2} Q_i^2. \tag{6}$$

As an energy conversion unit, a hydraulic motor converts the oil pressure in the hydraulic system to the mechanical energy so that the expansion pressure energy may be turned into the torque to the generator. The hydraulic motor rotary speed and output torque may be calculated by the following equations:

$$\begin{cases} n = \dfrac{Q_e}{q} \eta_v, \\ T_n = \dfrac{\Delta P_e q}{2\pi} \eta_m. \end{cases} \tag{7}$$

where: n represents the hydraulic motor rotary speed; Q_e represents the flux of hydraulic motor; q represents the displacement of the hydraulic motor; η_v represents the volume efficiency of the hydraulic motor; T_n represents the output torque of the hydraulic motor; and η_m represents the mechanical efficiency of the hydraulic motor.

The generator is driven by a hydraulic motor so that its voltage and torque shall meet the following equations:

$$\begin{cases} V_e = k_v w, \\ T_n = J\ddot{w} + k_t I, \end{cases} \tag{8}$$

where: V_e represents the induction electromotive force; k_v represents the back electromotive force constant; w represents the rotate speed of the generating rotor ($w = 2\pi n$); T_n represents the output torque of the hydraulic motor; J represents the rotary inertia of the generating rotor; k_t represents the torque constant of the generator; and I represents the inductive current.

The induction electromotive force may be expressed as $V_e = IR$, where R represents the total resistance of the circuit. While ignoring the rotary inertia of the generating rotor, the following equation may be obtained:

$$\Delta P_e = \frac{4\pi^2 k_t k_v \eta_v}{q^2 \eta_m R} Q_e. \tag{9}$$

As above, the accumulator is primarily to absorb redundant oil due to contraction of the rod cylinder. By taking the initial and final charging states into account and ignoring any middle course, the compression pressure of the accumulator may be calculated based on the Boyle's law:

$$P_{acc} = P_0 \left[\frac{V_0}{V_0 - (A - A_a)s(t)} \right]^\kappa, \tag{10}$$

where: κ represents the gas polytrophic index; P_0 and V_0 represent the initial pressure and volume of the accumulator, respectively; and $s(t)$ represents the displacement of the piston at the time (t). When the input is sinusoidal wave ($s(t) = s_{max} \sin(2\pi ft)$, s_{max} denotes the maximum distance of piston), the linear friction loss of a hydraulic circuit during the expansion stroke may be expressed as:

$$\Delta P_p = \frac{128\rho l v_v}{\pi d^4} \cdot Q, \tag{11}$$

where: l and d represent the length and inner diameter of the oil pipe, respectively; v_v represents the fluid kinematic viscosity; and Q represents the flowrate of a hydraulic circuit.

While assuming the same flowrate in each hydraulic circuit during the expansion stroke, namely, $Q_1 = Q_2 = Q_e = Q$, then:

$$Q = A_a \cdot v. \tag{12}$$

From Eqs. (1)-(12), the expansion damping force may be calculated by:

$$F_c = \frac{\rho A_a^3 v^2}{2c_q^2}\left(\frac{1}{A_{c1}^2} + \frac{1}{A_{c2}^2}\right) + \frac{4\pi^2 k_t k_v \eta_v}{q^2 \eta_m R} A_a^2 \cdot v + \frac{128\rho l v_v}{\pi d^4} A_a^2 \cdot v$$
$$- P_0\left[\frac{V_0}{V_0 - (A - A_a)s(t)}\right]^\kappa \cdot A_r. \tag{13}$$

For verifying the accuracy of the mathematical model, the measured and simulated results in Fig. 3 were compared under the sinusoidal frequency and amplitude (1.67 Hz and 50 mm).

Owing to the oil transportation characteristics, there exists oil loss travel distortion in actual tests so that the damping force may be distorted locally as shown in the lower right corner of Fig. 3. However, performances of the damper may not be influenced distinctly. It is found based on the verification experiments that the actual maximum damping force is 4516 N and the simulated one is 4370 N with the difference of only 3.23 %; thus, the simulated and measured damping forces are in good agreement and the proposed HESA as a damper is reliable in the vehicle suspension system.

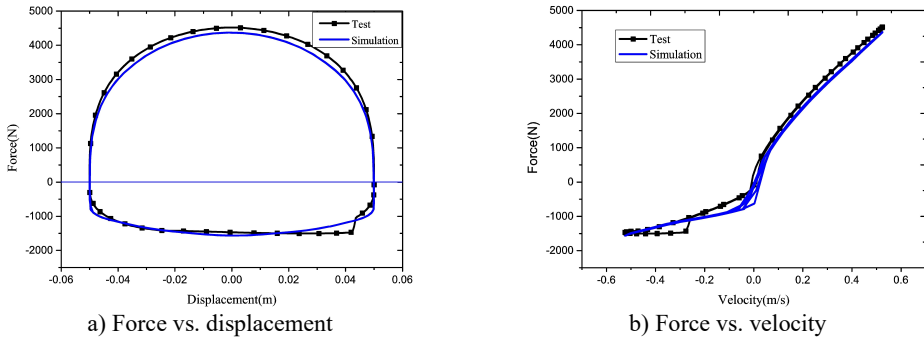a) Force vs. displacement b) Force vs. velocity
Fig. 3. Comparison of test and simulation results

Fig. 4. Traditional shock absorber and HESA test rig

Based on experiments of the HESA prototype without battery load, the compression damping

force was obtained, which is shown in Fig. 4. By combining the expansion damping force, the indicator diagram of HESA was presented. In comparison with those of the traditional shock absorber (TSA) under the same parameters, the results are shown in Fig. 5.

The comparison compression damping force results are in good agreement for the HESA and traditional shock absorber. On the other hand, the expansion damping forces are different under the same battery load.
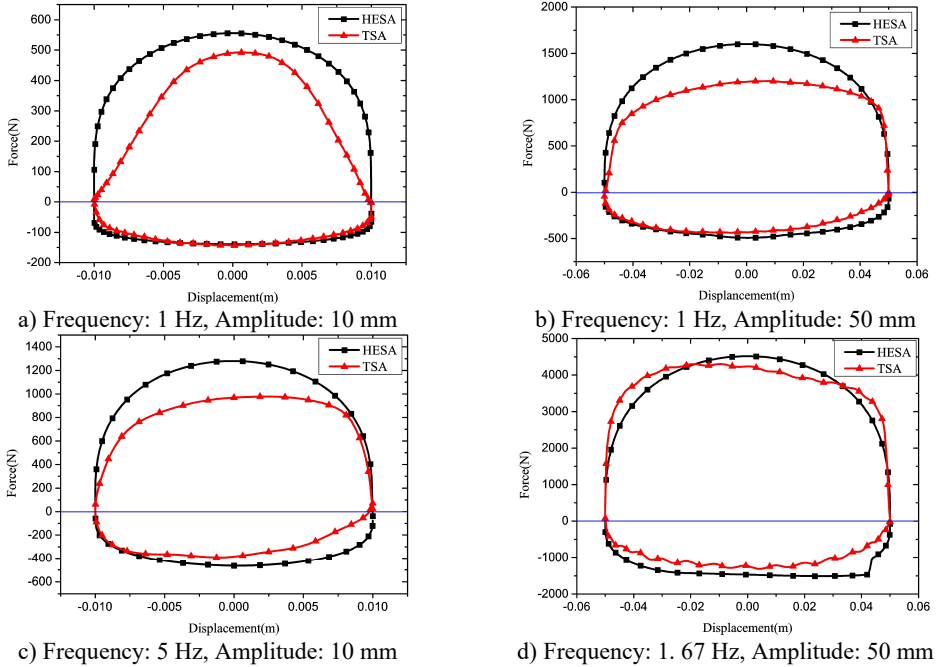

a) Frequency: 1 Hz, Amplitude: 10 mm

b) Frequency: 1 Hz, Amplitude: 50 mm

c) Frequency: 5 Hz, Amplitude: 10 mm

d) Frequency: 1. 67 Hz, Amplitude: 50 mm

Fig. 5. Comparison of indicator diagrams of HESA and TSA

2.2. HERS model

When the sprung mass allocation proportion is close to 1, the front and rear suspension systems are almost under independent vibration conditions. A quarter car was modeled to analyze the vehicle dynamics under certain road excitation conditions. As shown in Fig. 6, while the damping force of HESA is represented by F_a, the modeling dynamics may be easily written as:

$$\begin{pmatrix} m_b & 0 \\ 0 & m_w \end{pmatrix}\begin{pmatrix} \ddot{z}_2 \\ \ddot{z}_1 \end{pmatrix} + \begin{pmatrix} k_s & -k_s \\ -k_s & k_s + k_t \end{pmatrix}\begin{pmatrix} z_2 \\ z_1 \end{pmatrix} = \begin{pmatrix} F_a \\ k_t z_0 - F_a \end{pmatrix}, \tag{14}$$

where: m_b and m_w represent the sprung and unsprung masses, respectively; z_2 and z_1 represent the vertical displacements of sprung and unsprung masses, respectively; z_0 represents the road input displacement; k_s and k_t represent the suspension stiffness and the tire stiffness, respectively.

In comparison with a traditional suspension unit, a HESA includes an energy-harvesting shock absorber so that the vehicle ride comfort and the recovery of suspension vibration energy may be achieved.

3. Optimization of HERS

As above, a hydraulic-electricity energy regenerative suspension may recover energy as that of a traditional damper. Therefore, it is of great significance to study the equilibration between

energy-recovery and dynamic performances. The ride comfort and energy-recovery were optimized to achieve the optimal performances for the energy regenerative suspension unit.
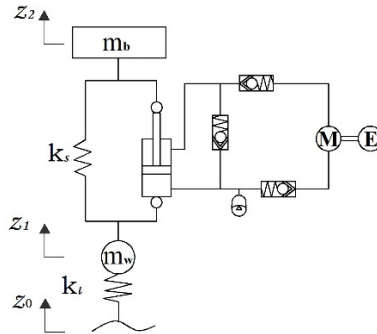

Fig. 6. Schematic diagram of a quarter car with a HESA

3.1. Optimization constraints

The hydraulic-electricity energy regenerative suspension unit shall ensure the satisfactory characteristics of comfort and handling performances so that the following constraints shall be satisfied.

3.1.1. Offset frequency

The sprung mass of a commercial vehicle is very large at full load so that the suspension offset frequency shall be relatively low and the operation stability of the vehicle may be reduced; therefore, the offset frequency n_1 should be restricted as:

$$n_1 = \frac{1}{2\pi}\sqrt{\frac{k_s}{m_b}}. \tag{15}$$

3.1.2. Suspension dynamic displacement

A suspension system is equipped between the frame and the axles, between which a safe distance primarily dependent on the reasonable parameters of HESA should be maintained to tolerate any vibration due to driving pavement excitation. Thus, the suspension dynamic displacement f_d is closely related to parameters of HESA and it is defined as:

$$f_d = z_2 - z_1. \tag{16}$$

3.1.3. Dynamic load of wheels

The dynamic load of wheels impacts the adhesion force between wheels and the road and is associated with the grip of the tires, which is vital to the handing stability and driving safety. When the RMS value of the tire dynamic load is constrained to $G/3$, the probability of wheel jumping off the ground is less than 0.15 %. Thus, the dynamic load of wheels should be constrained and the dynamic load coefficient is expressed by:

$$\xi = \frac{\sqrt{\frac{1}{T}\int_0^T F_d^2 dt}}{G}, \tag{17}$$

where: ξ represents the dynamic load coefficient; T represents the vibration time; F_d represents the dynamic loads of wheels; and G represents the static load of wheels.

3.2. Optimization objectives

The vibration acceleration of the sprung mass is broken into the vertical, longitudinal and lateral components at the centroid of the whole vehicle for studying the vehicle ride comfort, among which the vertical vibration acceleration in the center of the sprung mass is taken as the objective function J_1, whose RMS value is expressed by:

$$J_1 = a_w = \sqrt{\int_{0.5}^{80} W^2(f)G_a(f)df}, \tag{18}$$

where: a_w represents the RMS value of vertical vibration acceleration in the center of the sprung mass; $G_a(f)$ represents the acceleration power spectral density function; and $W(f)$ represents the frequency weighting function, which is expressed by:

$$W(f) = \begin{cases} 0.5, & 0.5 < f < 2, \\ f/4, & 2 < f < 4, \\ 1, & 4 < f < 12.5, \\ 12.5/f, & 12.5 < f < 80. \end{cases} \tag{19}$$

Besides, the ride performance, the recovered power should also be regarded as representation of the hydraulic-electricity energy regenerative suspension. The more recovered power is desired on the premise that the ride comfort may be guaranteed. The RMS value of the recovered power is taken as another objective function J_2, which is defined as:

$$J_2 = P_{rms} = \sqrt{\frac{1}{t} \int_0^t P(t)dt}, \tag{20}$$

where: P_{rms} represents the RMS value of the recovered power; and $P(t)$ represents the function of recovered power time with time, which may be determined based on testing results.

3.3. Analysis of influencing factors

HESA dominate performances of a hydraulic-electricity energy regenerative suspension unit. As for HESA in Fig. 2, the primary influencing factors are listed in Table 1.

Table 1. Primary influencing factors

Factor	Default value
Diameter of piston, D (mm)	50
Diameter of piston rod, D_r (mm)	20
Initial pressure of accumulator, P_0 (Pa)	2×10^6
Volume of accumulator, V_0 (L)	0.16
Hydraulic motor displacement, q (cc/rev)	5
Generator rotor resistance, R_0 (Ω)	2
Load current, I (A)	3

Because the HESA prototype is manufactured based on the traditional shock absorber of the target vehicle, diameters of the piston and the piston rod is taken into account in this study. Moreover, the initial pressure of accumulator $P_0(A)$, the volume of accumulator $V_0(B)$, the load

current $I(C)$, the internal resistance of the generator $R_0(D)$ and the hydraulic motor displacement $q(E)$ are regarded as primary influencing factors. The orthogonal tests were carried out to analyze their sensitivities.

For rational assessment of the level interval of each factor, the constraints were set up hereby in light of: (1) $1.3 \le n_1 \le 1.8$; (2) $f_d \le 65$; and (3) $\xi \le 1/3$; Class D road and the speed of 36 km/h are taken for calculation; and the standardized orthogonal table $L_{16}(4^5)$ is applied. By combining the characteristics of the hydraulic-electricity energy regenerative suspension unit, those influencing of factors were analyzed for the ride comfort and recovered suspension energy, whose orthogonal experiment design and results are listed in Table 2.

Based on the above orthogonal experiment results, the ranges of various factors were calculated, as in Tables 3 and 4, where K_i represents the arithmetic average of the evaluation index in i level test for each factor. The impact degree of any factor on the test evaluation index is reflected by its range; and the larger the range is, the greater the impact is.

Table 2. Design and results of orthogonal experiments

Test No.	A (Bar)	B (L)	C (A)	D (Ω)	E (cc/rev)	Results	
						a_w (m/s²)	P_{rms} (W)
1	10	0.12	1	0.5	3	0.8002	50.2437
2	10	0.16	3	1	5	0.9435	40.0227
3	10	0.2	4	1.5	7	0.8833	27.236
4	10	0.24	5	2	9	0.8155	38.3218
5	20	0.12	3	1.5	9	0.7953	48.4565
6	20	0.16	1	2	7	0.7582	26.4632
7	20	0.2	5	0.5	5	0.9797	113.0685
8	20	0.24	4	1	3	1.1382	61.9949
9	30	0.12	4	2	5	0.9211	97.8645
10	30	0.16	5	1.5	3	1.1972	140.1889
11	30	0.2	1	1	9	0.7522	20.7837
12	30	0.24	3	0.5	7	0.8207	66.7374
13	40	0.12	5	1	7	0.8855	87.4213
14	40	0.16	4	0.5	9	0.8198	64.0196
15	40	0.2	3	2	3	0.9979	127.5257
16	40	0.24	1	1.5	5	0.7713	40.0761

Table 3. Orthogonal experiment analysis of a_w

	A	B	C	D	E
K_1	0.861	0.851	0.77	0.855	1.033
K_2	0.918	0.93	0.889	0.93	0.904
K_3	0.923	0.903	0.941	0.912	0.837
K_4	0.869	0.886	0.969	0.873	0.796
Max	0.923	0.93	0.969	0.93	1.033
Min	0.861	0.851	0.77	0.855	0.796
Range	0.062	0.079	0.199	0.075	0.237

Table 4. Orthogonal experiment analysis of P_{rms}

	A	B	C	D	E
K_1	38.956	71.072	34.392	73.517	94.988
K_2	62.496	67.674	70.686	52.631	72.758
K_3	81.394	72.153	62.779	63.989	52.039
K_4	79.836	51.783	94.825	72.544	42.895
Max	81.394	72.153	94.825	73.517	94.988
Min	38.956	51.783	34.392	52.631	42.895
Range	42.438	20.37	60.433	20.886	52.093

The influencing tendency of performances of the reclaiming energy suspension unit may be obtained for each influencing factor based on above analysis results, as in Fig. 7.
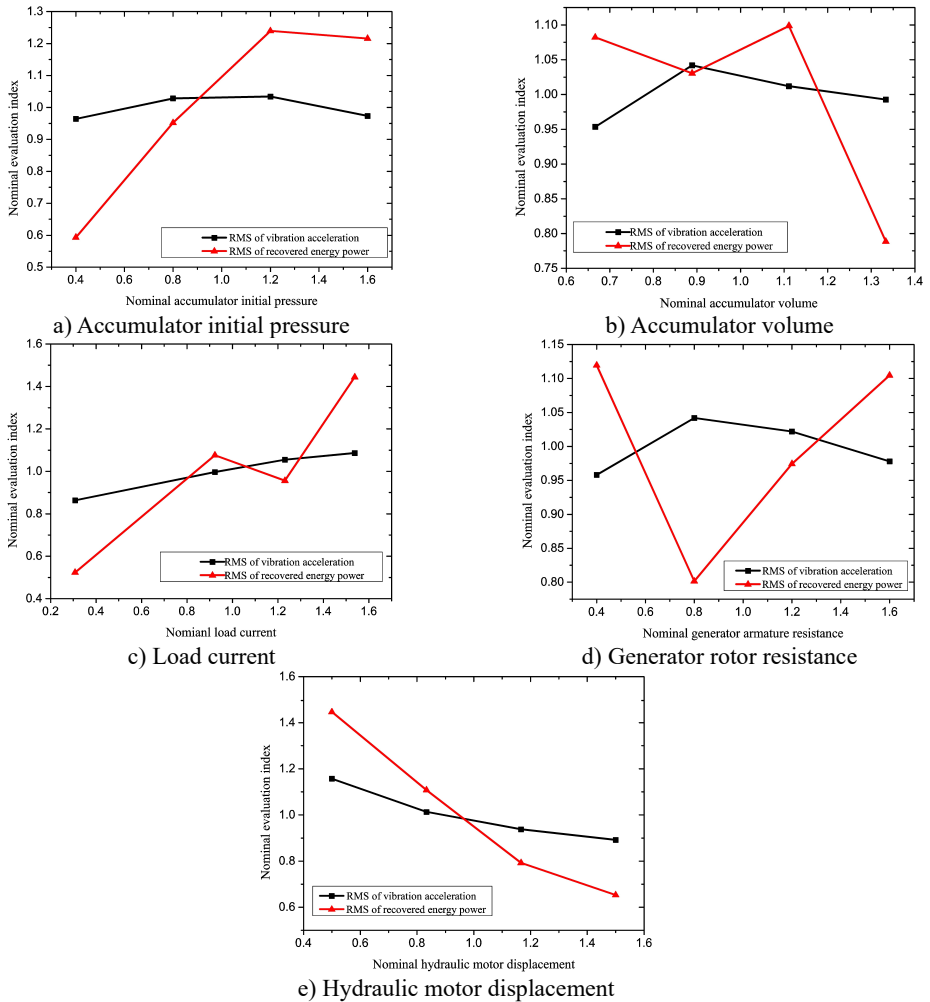

a) Accumulator initial pressure

b) Accumulator volume

c) Load current

d) Generator rotor resistance

e) Hydraulic motor displacement

Fig. 7. Diagrams of influencing factors

It is found from the above diagrams that those selected factors significantly impact the characteristics (especially the recovered power) of the reclaiming energy suspension unit; thus, they shall be taken into account to optimize performances of the hydraulic-electricity energy regenerative suspension unit, whose variable ranges are shown in Table 5.

Table 5. The range of variables value

	Initial	Minimum	Maximum
Accumulator initial pressure, P_0 (Pa)	2×10^6	$1\text{x}10^6$	5×10^6
Accumulator volume, V_0 (L)	0.16	0.12	0.24
Load current, I (A)	3	1	10
Generator rotor resistance, R_0 (Ω)	2	0. 5	5
Hydraulic motor displacement, q (cc/rev)	5	3	15

The optimization model may be expressed by:

find $\mathbf{X} = [P_0, V_0, I, R_0, q]$,

minimize $F_1(\mathbf{X}) = J_1$,

maximize $F_2(\mathbf{X}) = J_2$,

subject to $\begin{cases} \mathbf{X}_{min} \leq \mathbf{X} \leq \mathbf{X}_{max}, \\ n_{min} \leq n_1 \leq n_{max}, \\ f_d \leq 65, \\ \xi \leq 1/3, \end{cases}$ (21)

where: $\mathbf{X}_{min}$ and $\mathbf{X}_{max}$ represent the minimum and maximum of each design variable, respectively.

4. Optimization and result analysis

For optimizing comprehensive performances of the hydraulic-electricity energy regenerative suspension unit, analysis was carried out according to the following procedures in Fig. 8.
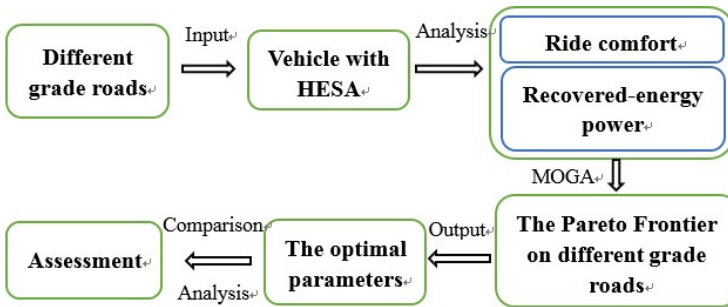
Fig. 8. Analysis process diagram

4.1. Road excitation input

The road excitation is a primary external input for any suspension system. The random road profile is generated by Gaussian white noise passing through a first order filter [20] in this study:

$$\dot{z}_0 = -2\pi f_0 \cdot z_0 + 2\pi n_0 \cdot w(t) \cdot \sqrt{G_q(n_0) \cdot u},$$ (22)

where: u is the vehicle speed; $w(t)$ is the zero-mean Gaussian white noise input with intensity 1 in time domain; f_0 is the low cut-off frequency, $f_0 = 0.1$ Hz hereby; and $G_q(n_0)$ is the road roughness coefficient, whose geometric mean values are listed in Table 6.

It is known from Eq. (22) that z_0 correlates closely with the vehicle velocity. The velocity varies from 10 m/s to 30 m/s in this study.

Table 6. Classification of road roughness

Road level	Geometric mean value of $G_q(n_0)$ / (10^{-6} m^3)
A	16
B	64
C	256
D	1024

4.2. Optimal design

Based on our optimization model, the sobol sequence was selected to 30 initial points in the variable range. An improved non-dominated ranking based MOGA (MOGA-II) was used to

perform the optimization process [21]. Since the design evaluation is very fast, a high number of generations was taken as 300 in this study. According to the recommended range, the probabilities of directional cross-over, selection and mutation were taken as 0.5, 0.05 and 0.1, respectively. DNA string mutation ratio was taken as 0.05. Thus, optimization results are shown in Fig. 9.
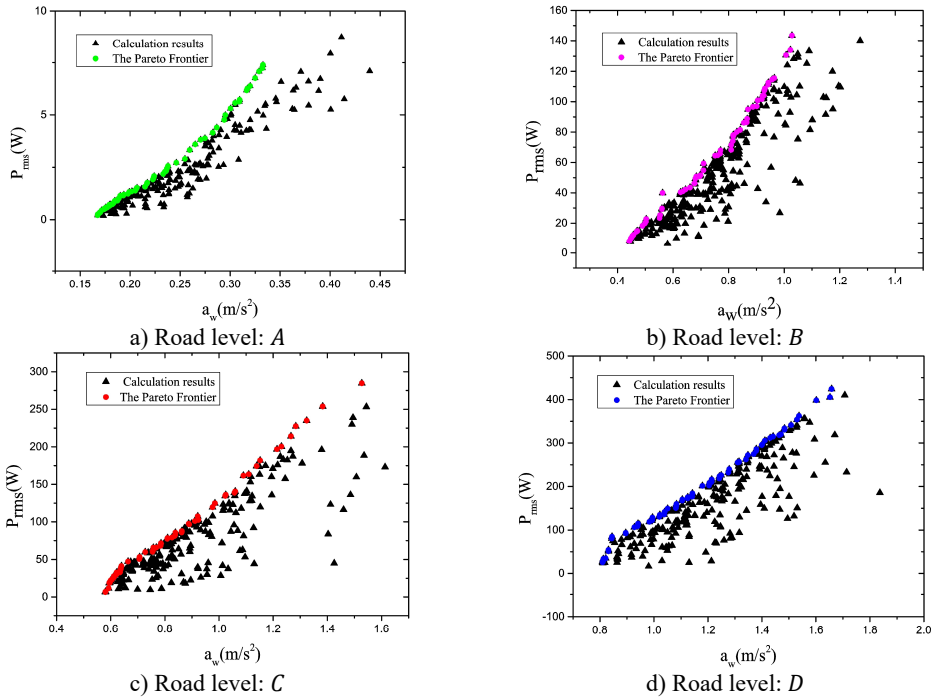

a) Road level: *A*

b) Road level: *B*

c) Road level: *C*

d) Road level: *D*

Fig. 9. Optimization results for different grade roads

It is found from Fig. 9 that the Pareto Frontier occurs for various grade roads; and the relationship (a_w vs. P_{rms}) may be obtained; in addition, the greater the acceleration RMS value is the more energy may be recycled within the same velocity context.
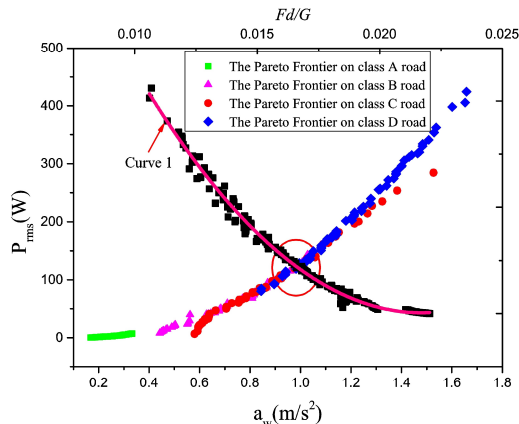
Fig. 10. Optimized Pareto frontier

The relationship (a_w vs. P_{rms}) in Fig. 10 reflect the monotone effect so that the tire dynamic load shall be introduced in the optimal design, in which the fitted curve 1 characterize the relation (P_{rms} vs. F_d/G); moreover, the intersection area was taken as the optimal solution range to

tolerate a small dynamic load. The optimal design was in Table 7.

Table 7. The main influencing factors

| Factors	Optimal design
Initial pressure of accumulator, P_0 (Pa)	3.4×10^6
Volume of accumulator, V_0 (L)	0.18
Hydraulic motor displacement, q (cc/rev)	5
Generator rotor resistance, R_0 (Ω)	2.5
Load current, I (A)	2

4.3. Comparative analysis

In view of the above optimal solution, comparison and analysis were carried out to ride comfort effects for the energy regenerative suspension unit and the traditional one under different random pavements, whose results are shown in Table 8.

Table 8. Comparative analysis results

Road level	Velocity (m/s)	Energy regenerative suspension		Traditional suspension
		P_{rms} (W)	a_w (m/s²)	a_w (m/s²)
A	10	4.671	0.188	0.298
	20	8.351	0.266	0.371
	30	11.562	0.326	0.422
B	10	14.433	0.376	0.467
	20	24.180	0.532	0.605
	30	33.862	0.651	0.715
C	10	24.323	0.532	0.603
	20	44.657	0.752	0.810
	30	69.098	0.921	0.972
D	10	44.880	0.752	0.810
	20	96.899	1.063	1.119
	30	159.207	1.303	1.367

In comparison with that of the traditional suspension unit, the optimized reclaiming energy suspension unit brings about marginally improved ride comfort. Moreover, a part of vibration energy is recovered by HESA, as in Fig. 11.
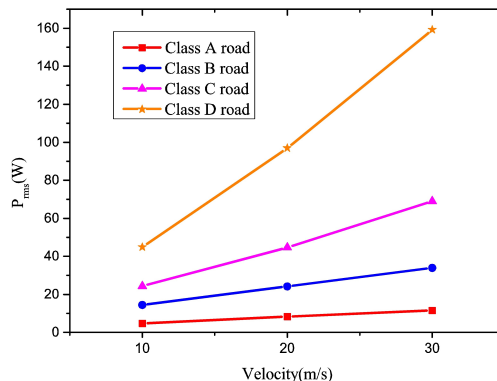
Fig. 11. Recovery power vs. velocity

For performance of ride comfort of the energy regenerative suspension unit, the amplitude-frequency characteristic was analyzed under a step excitation including the body acceleration, the suspension dynamic displacement and the relative dynamic load of wheels,

whose results are given in Figs. 12, 13 and 14.

It may be known based on the amplitude-frequency characteristic of the body acceleration that their acceleration responses are basically the same within the range $(0.1, f_2)$ Hz; whereas, the acceleration response is smaller for the energy regenerative suspension unit while the excited frequency is more than f_2. Especially, it is of great significance to improve the ride comfort under high frequency excitation conditions.
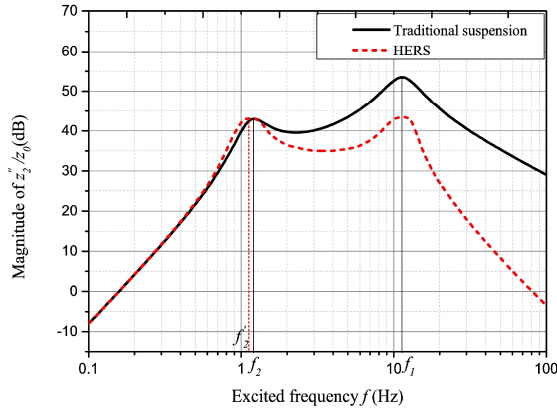

Fig. 12. Amplitude-frequency characteristic of $\ddot{z}_2/z_0$
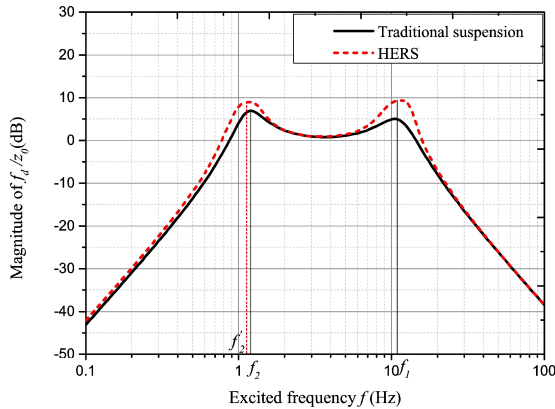
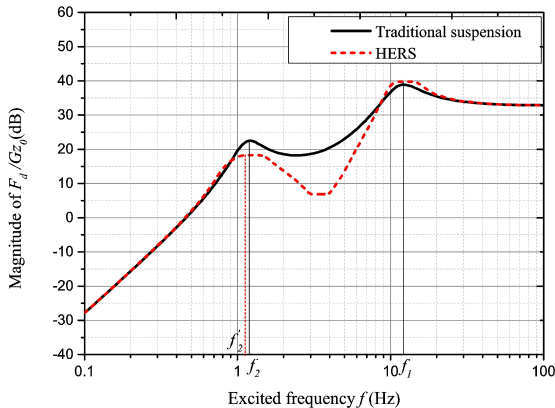**Fig. 13.** Amplitude-frequency characteristic of f_d/z_0

Fig. 14. Amplitude-frequency characteristic of F_d/Gz_0

Their amplitude-frequency characteristics include almost the consistent suspension dynamic displacement responses; on the other hand, the dynamic deflection response is intensified to a certain extent around two peak frequencies.

The tire dynamic load is dominant for choice of the optimal solution. It may be seen from Fig. 14 that the dynamic load response is improved between the two peak frequencies, which are very important for improving the driving stability.

The two peak frequencies represent the resonance frequencies of the sprung mass and the unsprung mass frequencies, respectively. The HESA energy recovery system may relieve the suspension effect so that the resonance frequency of the sprung mass shall be decreased correspondingly. Since the tire stiffness is much more than the suspension stiffness, the resonance frequency of the unsprung mass does not change significantly.

In contrast, the damping characteristics of a traditional shock absorber are given in Table 9. Based on the optimal parameters, different damping characteristic curves may be obtained under various battery load currents, as in Fig. 15. In comparison with the traditional shock absorber, the HESA may be utilized to control the recovery resistance by adjusting the load current, which is an important measure to perform control of the HERS.

Table 9. Damping characteristics of shock absorber

Speed (m/s)	Recovery resistance (N)	Compression resistance (N)
0.052	1722±374	191±78
0.131	2995±629	448±130
0.262	3511±557	620±149
0.393	4155±647	843±187
0.524	4847±757	1212±252
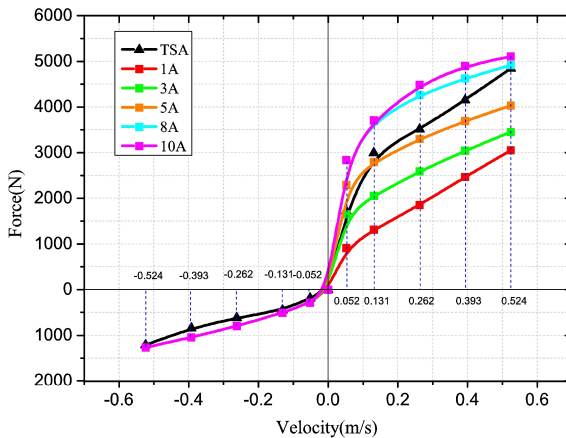
Fig. 15. Damping characteristic curves of HESA

5. Conclusions

The characteristics (including ride performance and energy-recovery) of the hydraulic-electricity energy regenerative suspension unit were analyzed to compromise between the energy-recovery and dynamic performances. The RMS value of the sprung mass vibration acceleration and the recovered power were optimized under constraints (such as natural frequency, dynamic displacement, and dynamic load of wheels) and different road excitation conditions. The dynamic loads are taken into account to determine the optimal solution of HESA. The analysis results indicate that the ride comfort of the optimized reclaiming energy suspension unit may be improved remarkably so that it shall be quite suitable for the vehicle driving. In addition, it may be used to control the suspension effect since a part of vibration energy is recycled.

In summary, multi-objective optimization was carried out to optimized parameters of HESA and compromise between the energy-recovery and dynamic performances; thus, the HERS may be put into optimal operation; moreover, this study lays a firm foundation for control of energy regenerative suspension units.

Acknowledgements

References

[1] Energy Information Administration Basic Petroleum Statistics, http://www.eia.doe.gov/basics/.
[2] Economic Report of the President, http://www.whitehouse.gov/cea/ch6-erp07.pdf.
[3] Advanced Technologies and Energy Efficiency, http://www.fueleconomy.gov/FEG/atv.shtml.
[4] Karnopp D. Permanent magnet linear motors used as variable mechanical dampers for vehicle suspensions. Vehicle System Dynamics, Vol. 18, Issue 4, 1989, p. 187-200.
[5] Hsu P. Power recovery property of electrical active suspension systems. Energy Conversion Engineering Conference, Proceedings of the 31st Intersociety, Vol. 3, 1996, p. 1899-1904.
[6] Suda Y., Nakadai S., Nakano K. Hybrid suspension system with skyhook control and energy regeneration (development of self-powered active suspension). Vehicle System Dynamics, Vol. 29, Issue 1, 1998, p. 619-634.
[7] Nakano K., Suda Y., Nakadai S., Koike Y. Anti-rolling system for ships with self-powered active control. JSME International Journal Series C Mechanical Systems, Machine Elements and Manufacturing, Vol. 44, Issue 3, 2001, p. 587-593.
[8] Nakano K., Suda Y., Nakadai S. Self-powered active vibration control using a single electric actuator. Journal of Sound and Vibration, Vol. 260, Issue 2, 2003, p. 213-235.
[9] Kawamoto Y., Suda Y., Inoue H., Kondo T. Electro-mechanical suspension system considering energy consumption and vehicle manoeuvre. Vehicle System Dynamics, Vol. 46, Issue 1, 2008, p. 1053-1063.
[10] Chen C., Liao W. H. A self-sensing magnet orheological damper with power generation. Smart Materials and Structures, Vol. 21, Issue 2, 2012, p. 025014.
[11] Jones W. D. Easy ride: Bose Corp. uses speaker technology to give cars adaptive suspension. IEEE Spectrum, Vol. 42, Issue 5, 2005, p. 12-14.
[12] Zuo L., Scully B., Shestani J., Zhou Y. Design and characterization of an electromagnetic energy harvester for vehicle suspensions. Smart Materials and Structures, Vol. 19, Issue 4, 2010, p. 045003.
[13] Kawamoto Y., Suda Y., Inoue H., Kondo T. Modeling of electromagnetic damper for automobile suspension. Journal of System Design and Dynamics, Vol. 1, Issue 3, 2007, p. 524-535.
[14] Zhang Y., Huang K., Yu F., Gu Y., Li D. Experimental verification of energy-regenerative feasibility for an automotive electrical suspension system. IEEE International Conference on Vehicular Electronics and Safety, 2007, p. 1-5.
[15] Choi S. B., Seong M. S., Kim K. S. Vibration control of an electrorheological fluid-based suspension system with an energy regenerative mechanism. Proceedings of the Institution of Mechanical Engineers, Part D: Journal of Automobile Engineering, Vol. 223, Issue 4, 2009, p. 459-469.
[16] Li Z., Brindak Z., Zuo L. Modeling of an electromagnetic vibration energy harvester with motion magnification. ASME International Mechanical Engineering Congress and Exposition, 2011, p. 285-293.
[17] Liu S., Wei H., Wang W. Investigation on some key issues of regenerative damper with rotary motor for automobile suspension. International Conference on Electronic and Mechanical Engineering and Information Technology, Vol. 3, 2011, p. 1435-1439.
[18] Fang Z., Guo X., Xu L., Zhang H. Experimental study of damping and energy regeneration characteristics of a hydraulic electromagnetic shock absorber. Advances in Mechanical Engineering, Vol. 5, 2013, p. 943528.

[19] **Zhang H., Guo X., Xu L., Hu S., Fang Z.** Parameters analysis of hydraulic-electrical energy regenerative absorber on suspension performance. Advances in Mechanical Engineering, Vol. 6, 2014, p. 836502.

[20] **Kaldas M., Henze R., Küçükay F.** Improvement of heavy vehicles ride and braking performance via combined suspension and braking systems control. SAE International Journal of Materials and Manufacturing, Vol. 4, Issue 1, 2011, p. 535-552.

[21] **Fonseca C. M., Fleming P. J.** Genetic algorithms for multi-objective optimization: formulation discussion and generalization. ICGA, Vol. 93, 1993, p. 416-423.
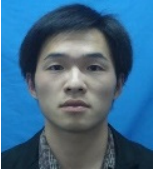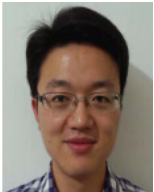
Bian Gong received M.S. degree in Automotive Engineering Institute from Wuhan University of Technology, Wuhan, China, in 2014. Now he carries out his Ph.D. research in the area of energy recovery and vehicle dynamics in Wuhan University of Technology.

Xuexun Guo received Ph.D. degree in Automotive Engineering Institute from Beijing Institute of Technology, Beijing, China, in 1995. Now he works at Wuhan University of Technology. His current research interests include control, vehicle dynamics and energy recovery.

Sanbao Hu received Ph.D. degree in Mechanical Science and Engineering Institute from Huazhong University of Science and Technology, Wuhan, China, in 2011. Now he works at Wuhan University of Technology. His current research interests include vibration, dynamics and optimization.

Zhigang Fang received Ph.D. degree in Automotive Engineering Institute from Wuhan University of Technology, Wuhan, China, in 2013. Now he works at Wuhan University of Technology. His current research interests include vehicle dynamics and energy recovery.